

Identification of Dy³⁺ /Dy²⁺ as electron trap in persistent phosphors

Joos, J. J.; Korthout, K.; Amidani, L.; Glatzel, P.; Poelman, D.; Smet, P. F.;

Originally published:

July 2020

Physical Review Letters 125(2020), 033001

DOI: <https://doi.org/10.1103/PhysRevLett.125.033001>

Perma-Link to Publication Repository of HZDR:

<https://www.hzdr.de/publications/Publ-31060>

Release of the secondary publication
on the basis of the German Copyright Law § 38 Section 4.

Identification of $\text{Dy}^{3+}/\text{Dy}^{2+}$ as electron trap in persistent phosphors

JONAS J. JOOS^{1,2,†}, KATLEEN KORTHOUT^{1,2}, LUCIA AMIDANI^{3,‡}, PIETER GLATZEL³, DIRK POELMAN^{1,2}, PHILIPPE F. SMET^{1,2,†}

¹ LumiLab, Department of Solid State Sciences, Ghent University, Gent, Belgium

² Center for Nano- and Biophotonics (NB Photonics), Ghent University, Gent, Belgium

³ European Synchrotron Radiation Facility (ESRF), Grenoble, France

[†] E-mail: jonas.joos@UGent.be, philippe.smet@UGent.be

[‡] Current affiliation: Helmholtz-Zentrum Dresden-Rossendorf, Dresden, Germany

Abstract

A long-standing issue in persistent luminescence is settled by providing direct evidence that Dy^{3+} is the main electron trap in $\text{Sr}_4\text{Al}_{14}\text{O}_{25}:\text{Eu},\text{Dy}$ by combining laser excitation with X-ray spectroscopy. A reversible electron transfer is demonstrated, controlled by light and showing the same kinetics as the persistent luminescence. Exposure to violet light induces charging by oxidation of the excited Eu^{2+} while Dy^{3+} is simultaneously reduced. Oppositely, detrapping of Dy^{2+} occurs at ambient temperature or by infrared illumination, yielding afterglow or optically stimulated luminescence, respectively.

Luminescent materials or phosphors are crucial for various technological applications, ranging from environmentally friendly lighting^{1,2} to specialized applications in medicine and optoelectronics³⁻⁷. A subclass of luminescent materials are those that feature energy storage capabilities. For these compounds, not all of the energy absorbed upon excitation is immediately emitted as photoluminescence (PL). A fraction is used to transfer a charge carrier from the luminescent center to a so-called trap, generating a metastable state.

The lifetime of these metastable states can range over many orders of magnitude (quantified by the so-called trap depth), leading to very diverse applications. The long lifetimes of deep traps is exploited to date minerals or archeological artifacts, or for dosimeters, *e.g.* in medical imaging plates where red or infrared (IR) light is used to detrap charge carriers and induce the radiative decay of the luminescence activator, a process called optically stimulated luminescence (OSL)^{8,9}. For luminescent materials with more shallow traps, ambient temperature can be sufficient to slowly thermally deplete the traps (in minutes to hours), giving rise to the process of long afterglow or persistent luminescence¹⁰⁻¹³. This process can be accelerated by heating the phosphor, giving rise to thermoluminescence (TL), the analysis of which allows to experimentally extract information on trap depths or trap depth distributions^{14,15}. Afterglow materials hold the promise of new applications such as glow-in-the-dark traffic signalization¹⁶, damage monitoring¹⁷, radiation-free medical imaging^{3,18}, theranostics^{19,20}, cell characterization²¹ or nanothermometry²². The storage capabilities need nevertheless to be improved

in order to enable these advanced applications and important steps are yet to be taken in the optimization of existing materials and for the development of new ones^{12,13}.

In the 1990's it was found that some Eu^{2+} based phosphors acquire intense persistent luminescence upon codoping with a trivalent lanthanide ion (Ln^{3+}), often Dy^{3+} ²³. This triggered the discovery of a group of phosphors that, 25 years after the initial discovery, can still be regarded as state-of-the-art. Among them, the strontium aluminates ($\text{SrAl}_2\text{O}_4:\text{Eu}^{2+},\text{Dy}^{3+}$ and $\text{Sr}_4\text{Al}_{14}\text{O}_{25}:\text{Eu}^{2+},\text{Dy}^{3+}$) and the silicate $\text{Sr}_2\text{MgSi}_2\text{O}_7:\text{Eu}^{2+},\text{Dy}^{3+}$ take the most prominent places^{10,12}. As the trapping capacity is significantly increased upon Dy^{3+} addition, it is tempting to identify the trivalent codopant as a trap. To date, no hard evidence has however been found that confirms or rejects a valence state change for Dy^{3+} . The reason for this standstill is the difficulty to detect such transient phenomenon in common structural and optical experiments, and the intrinsic complexity of these materials, making theoretical studies scarce and hard to correlate with experiments such as TL^{24,25}.

TL experiments have suggested that distributions of trap depths are present, rather than one discrete trap^{15,26}. However, TL does not infer the chemical nature of the traps, and the distribution can be due to multiple intrinsic defects that induce trapping²⁷, but equally well to multiple nonequivalent Dy^{3+} centers in the crystal²⁸ distributed at different distances from the Eu^{2+} activator²⁹. Detailed experimental studies of $\text{SrAl}_2\text{O}_4:\text{Eu}^{2+},\text{Dy}^{3+}$ suggest that trapping is local, *i.e.* close to the Eu^{2+} activator rather than a delocalization

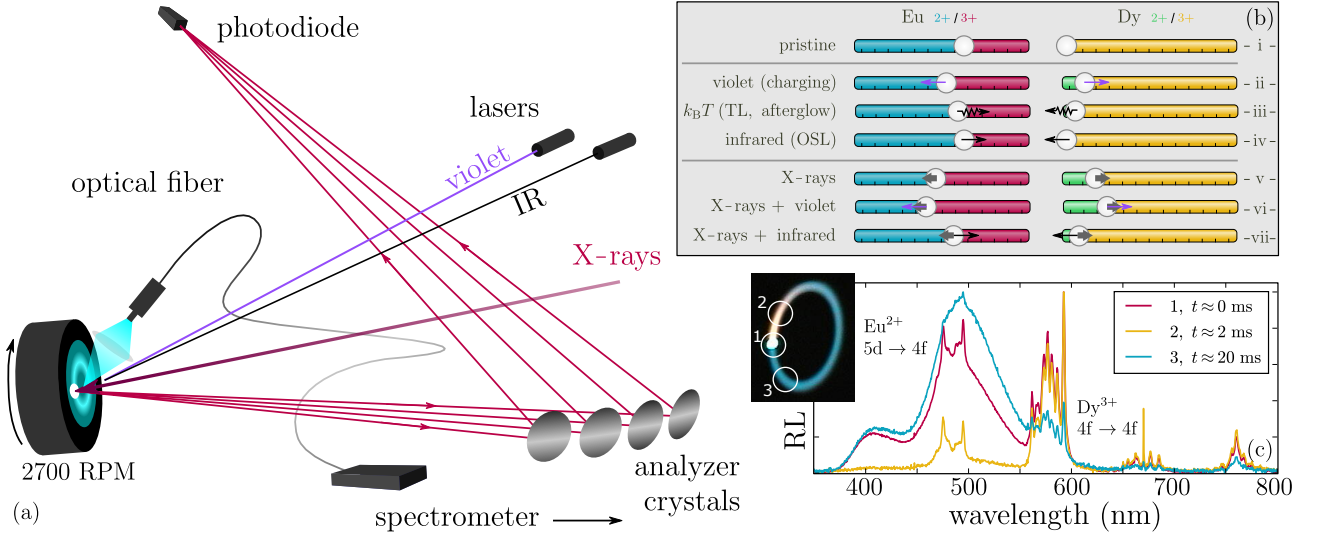


Figure 1 – Schematic representation of the experimental setup (a): monochromatic X-rays strike the rotating sample, the X-ray fluorescence is analyzed by a spectrometer in Rowland geometry, using an array of spherically bent crystal analyzers and an avalanche photodiode (APD). The sample is irradiated by violet or IR lasers and the radioluminescence (RL) is recorded. The schematic representation in (b) illustrates how light of different wavelengths, temperature and X-rays induce electron (e^-) transfer and hence affect the Eu^{2+} - Eu^{3+} (blue-red) and Dy^{2+} - Dy^{3+} (green-yellow) equilibria in the phosphor. Normalized radioluminescence spectra (c), measured on three different spots on the rotating sample are displayed, featuring $\text{Eu}^{2+} 4f^6 5d^1 \rightarrow 4f^7$ broadband and $\text{Dy}^{3+} 4f^9 \rightarrow 4f^9$ (${}^4F_{9/2} \rightarrow {}^6H_J$ ($2J = 15, 13, 11, 9$)) line emissions.

of the electron towards the conduction band²⁶. A limited number of X-ray absorption spectroscopy (XAS) studies have been performed on Eu^{2+} , Ln^{3+} codoped aluminates and silicates in the past^{30–35}. Most studies failed to find reversible valence state changes, except for Korthout *et al.* who uncovered a partial oxidation of Eu^{2+} to Eu^{3+} in $\text{SrAl}_2\text{O}_4:\text{Eu}^{2+}, \text{Dy}^{3+}$ ³⁴. Exposure to X-rays does not only lead to radioluminescence (RL) from Eu^{2+} but also to charge trapping, as witnessed by the slow increase of RL intensity (the so-called charging) after switching on the X-ray beam and by the afterglow when switching off the X-ray beam. Thermal cleaning of traps was used to ensure that the electron transfer was reversible, *i.e.* that the observed oxidation was not due to a degradation process. This confirmed that indeed an electron is released from the Eu^{2+} ion during the charging (trapping) process, but no convincing information could be extracted on where it is trapped³⁴. Carlson *et al.* recorded oxidation of Eu^{2+} in $\text{Sr}_2\text{MgSi}_2\text{O}_7:\text{Eu}$, but on a much longer timescale (hours) than the typical charging (seconds-minutes^{26,34}), indicating that this was presumably caused by degradation, rather than the filling of traps³².

In this letter, we report a novel experimental investigation where the valence state changes of both Eu and Dy in $\text{Sr}_4\text{Al}_{14}\text{O}_{25}:\text{Eu}^{2+}, \text{Dy}^{3+}$ persistent phosphors are recorded via Resonant Inelastic X-ray Scattering (RIXS, see Fig. 1(a)). It is found that a fraction of the Dy^{3+} is reduced to Dy^{2+} along with the oxidation of Eu^{2+} to Eu^{3+} , and that this reversible electron transfer is indeed responsible for the persistent luminescence.

The situation for a pristine Eu,Dy codoped persistent phosphor is represented in Fig. 1b(i), where Eu^{2+}

and Eu^{3+} coexist with Dy^{3+} . Charging by blue to ultraviolet light (Fig. 1b(ii)) or X-rays (Fig. 1b(v)) causes a part of the Eu^{2+} to be oxidized, while the redox partner, Dy^{3+} or another defect, gets reduced. This metastable state is long-lived and is slowly depleted at room temperature in case of persistent phosphors (Fig. 1b(iii)), giving rise to afterglow or TL when the electron is transferred back to the Eu center. Infrared light has a similar effect by electronically exciting the trapped electron, giving rise to OSL (Fig. 1b(iv)).

When probing the sample with X-rays, the density of trapped charges can additionally be perturbed by illuminating the sample with violet or IR lasers as illustrated in Fig. 1. This gives rise to the situations represented schematically in Fig. 1b(vi and vii) where the effect of the lasers is superimposed on the effect of the X-rays. The use of the external light sources hence allowed us to affect a fraction of the charges and create a differential effect on top of the unavoidable charging induced by X-rays.

Additionally to laser illumination controlling the electron transfer, the sample was mounted on a rotating stage and spinned during the measurements. Rotating the sample allows to probe a larger sample volume and reduce the photon per unit volume per unit time. The main advantage is that when X-rays hit the sample, the time to reach a steady state (the equilibrium between the trapping effect of X-rays and the detrapping processes) is hugely enlarged, passing from a few ms to tens of seconds. As a consequence, the time evolution of the charging process as induced by X-rays becomes measurable. Finally, we were able to connect the X-ray measurements with the luminescence processes by collecting the RL emitted by the

sample under X-ray illumination. The parallel analysis of the two data sets was fundamental to ensure that the observation for Eu and Dy are indeed connected to the persistent luminescence process.

Our experiments were conducted on commercial $\text{Sr}_4\text{Al}_{14}\text{O}_{25}:\text{Eu,Dy}$ powders at beamline ID26 of the European Synchrotron Radiation Facility (ESRF) in Grenoble, France^{36,37}. The sample was diluted in boron nitride (BN), pressed to a pellet and mounted on a rotating sample stage (2700 RPM). The Ln L_{III} absorption edges were used to probe the oxidation states of Eu and Dy. The rotating sample was positioned in the X-ray beam (see Fig. 1). The incident photon energy was scanned across the Eu and Dy L_{III} edge. The maximum of the characteristic $L_{\alpha 1}$ emission was selected by an X-ray emission spectrometer based on Rowland geometry, resulting in High Energy Resolution Fluorescence Detected X-ray Absorption Near Edge Structure (HERFD-XANES) spectra. For this experiment, the main advantage of using the HERFD mode to collect XANES is its superior energy resolution which increments the sensitivity of the technique to small spectral variations^{38–40}. More technical details about the experimental setup are given in the *Supplementary Information*.

The spinning sample allows to record spectral changes on a ms timescale as shown by Fig. 1(c). The inset displays a picture of the clockwise rotating (16 °/ms) sample under continuous X-ray irradiation. The color of the luminescence changes, depending on the position, and hence on the time after irradiation. This is analyzed in detail by continuously recording the luminescence spectra. The figure shows spectra that were recorded at different positions (1, 2, 3) on the spinning pellet, corresponding to delays of 0 ms, 2 ms and 20 ms after irradiation, respectively. Upon X-ray irradiation (position 1), different spectral components are clearly visible: the blue-green broadband $4f^65d^1 \rightarrow 4f^7$ emissions from Eu^{2+} in $\text{Sr}_4\text{Al}_{14}\text{O}_{25}$ peaking around 495 nm^{41,42} as well as characteristic Dy^{3+} inter- $4f^9$ transitions, predominantly in the yellow. The first few milliseconds after irradiation (position 2), the parity and spin-allowed Eu^{2+} emission already decayed (order of 1 μs) and the slow-decaying Dy^{3+} emission dominates the spectrum. The Dy^{3+} decay is clearly visible on the picture in Fig. 1. After 20 ms (position 3), also the excited Dy^{3+} ions have largely decayed and the afterglow remains, showing a dominant Eu^{2+} $4f^65d^1 \rightarrow 4f^7$ emission. It is hence clear that the X-rays are indeed able to excite the persistent luminescence.

Figure 2(a) shows HERFD-XANES spectra, measured at the Eu L_{III} edge. These spectra feature two relatively sharp peaks, so-called white lines, that correspond to the resonant $2p^64f^N \rightarrow 2p^54f^N5d^1$ electronic transition of Eu^{2+} ($N = 7$, around 6.975 keV) and Eu^{3+} ($N = 6$, around 6.983 keV)^{44,45}. The characteristic 7-8 eV separation between Eu^{2+} and Eu^{3+} white lines, and more generally between Ln^{2+} and Ln^{3+} white lines^{43,46}, is often used to acquire quantitative and qualitative information about the concurrence

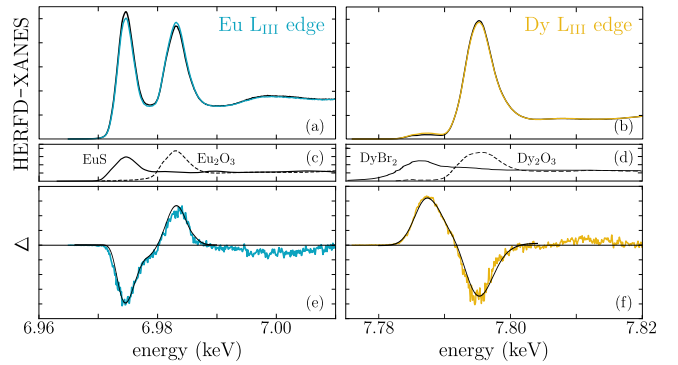


Figure 2 – High Energy Resolution Fluorescence Detected X-ray Absorption Near Edge Structure (HERFD-XANES) spectra for the Eu (a) and Dy (b) L_{III} edges upon violet (colored line) or IR (black line) irradiation, compared to conventional XANES of reference spectra for (c) EuS (EuII) and Eu_2O_3 (EuIII) and (d) Dy_2O_3 (DyIII) and DyBr_2 (DyII , adapted from⁴³), and the associated difference spectra, Δ , (colored lines) with their fit (black line) (e-f).

of lanthanide oxidation states^{44,45}.

It was previously found that Eu^{2+} oxidizes to Eu^{3+} in $\text{SrAl}_2\text{O}_4:\text{Eu,Dy}$ upon X-ray irradiation on the same timescale as the charging of the persistent luminescence³⁴. Therefore, it is clear that the X-rays, which are used as a probe for the lanthanide oxidation states, induce a net trapping effect, where a steady-state regime with a higher $[\text{Eu}^{3+}]:[\text{Eu}^{2+}]$ ratio, compared to a pristine sample, is established under irradiation (Fig. 1b(v)). In order to push this dynamic equilibrium in both directions, laser stimulation was applied on top of the X-ray irradiation: violet light to further increase $[\text{Eu}^{3+}]:[\text{Eu}^{2+}]$ (Fig. 1b(vi)) and IR light to provoke detrapping, counteracting the effect of the X-rays, thus lowering the $[\text{Eu}^{3+}]:[\text{Eu}^{2+}]$ ratio (Fig. 1b(vii)).

Figure 2(a) shows the effect of the laser stimulation. It is clear that the blue curve, for violet stimulation,

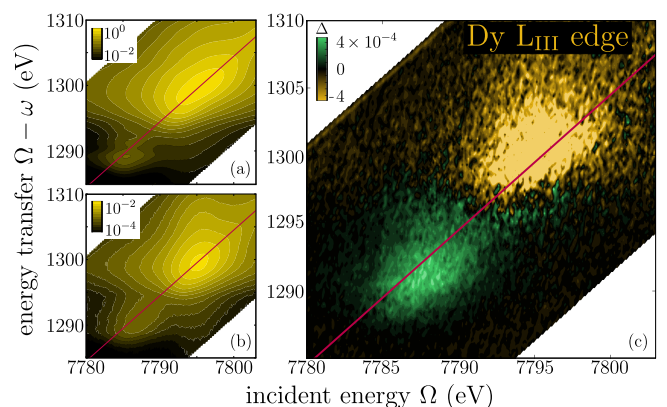
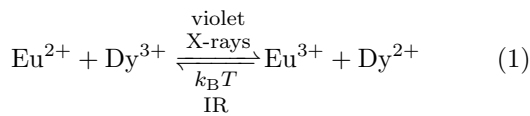


Figure 3 – RIXS planes of Dy_2O_3 (a) and $\text{Sr}_4\text{Al}_{14}\text{O}_{25}:\text{Eu,Dy}$ (b), and the difference of RIXS planes of $\text{Sr}_4\text{Al}_{14}\text{O}_{25}:\text{Eu,Dy}$, measured upon violet and IR illumination (c). The red straight line corresponds to a scan of the incident energy at fixed emission energy (HERFD-XANES). All planes measured at the Dy L_{III} edge.

presents a higher $[\text{Eu}^{3+}]:[\text{Eu}^{2+}]$ ratio than the black curve, for IR stimulation. Interestingly, a similar but opposite effect **on the same timescale** was found for the same experiment, performed at the Dy L_{III} edge. Figure 2(b) indicates that the amount of Dy³⁺ goes slightly down upon violet stimulation (yellow curve), compared to IR stimulation (black curve). Concurrently, a small increase of the spectral intensity in the region where the Dy²⁺ white line is expected can be observed. Figures 2(e-f) display the differences between the HERFD-XANES spectra, measured upon violet and IR stimulation, more clearly illustrating the valence changes.

The Dy²⁺ white line lies at lower energy than the Dy³⁺ white line, in the region where the Dy³⁺ pre-edge features are also observed (see Fig. 2(d)). The latter, which typically show a richer fine structure, are due to weakly allowed $2p^6 4f^9 \rightarrow 2p^5 4f^{10}$ transitions⁴⁷⁻⁵⁰. In our experiment, both features have a comparably low intensity. In order to confirm that the changes below the Dy³⁺ white line are indeed due to the creation of Dy²⁺, RIXS planes were measured under both illumination conditions and compared to RIXS planes of the pre-edge region (Fig. 3). The Dy³⁺ pre-edge structure is clearly seen in the RIXS plane of Dy₂O₃, but it is obscured for the phosphor sample. The difference of the violet and IR illuminated RIXS planes confirms that the spectral changes correspond to a decrease of the amount of Dy³⁺ and an increase of Dy²⁺: two broad bands are found, consistent with the rise of a Dy²⁺ white line, rather than with changes in the Dy³⁺ pre-edge region. This explains why the Dy³⁺ pre-edge structure is obscured for the phosphor sample as the X-rays inevitably create some Dy²⁺ in the phosphor (see also Fig. 1(b)).

These observations clearly prove the existence of the following photoinduced electron transfer



in accordance with the scheme in Fig 1(b). To obtain reliable estimates for the quantity of Eu and Dy that changes oxidation states, the HERFD-XANES spectra were fitted⁵¹⁻⁵³ with two Gaussians, one for each white line, and a smooth step function, representing the electronic transitions towards the dense set of unbound states, $2p^6 4f^N \rightarrow 2p^5 4f^N \phi^1$. Details about the fits are given in the *Supplementary Information* and the result for the difference spectra is shown in Figs. 2(e-f).

The area under the white line is associated with the concentration of Ln ions⁴³⁻⁴⁵. By exploiting that the total number of Ln ions remains constant throughout the experiment, it was verified that difference spectra of Fig. 2(e-f) correspond to 3% of all Eu and 2% of all Dy. Given the higher concentration of Dy in the phosphor (as verified by EDX⁵⁴, see *Supplementary Information*), quantitative agreement is found between the valence changes of Eu and Dy within the experimental uncertainties. This number is of the same order

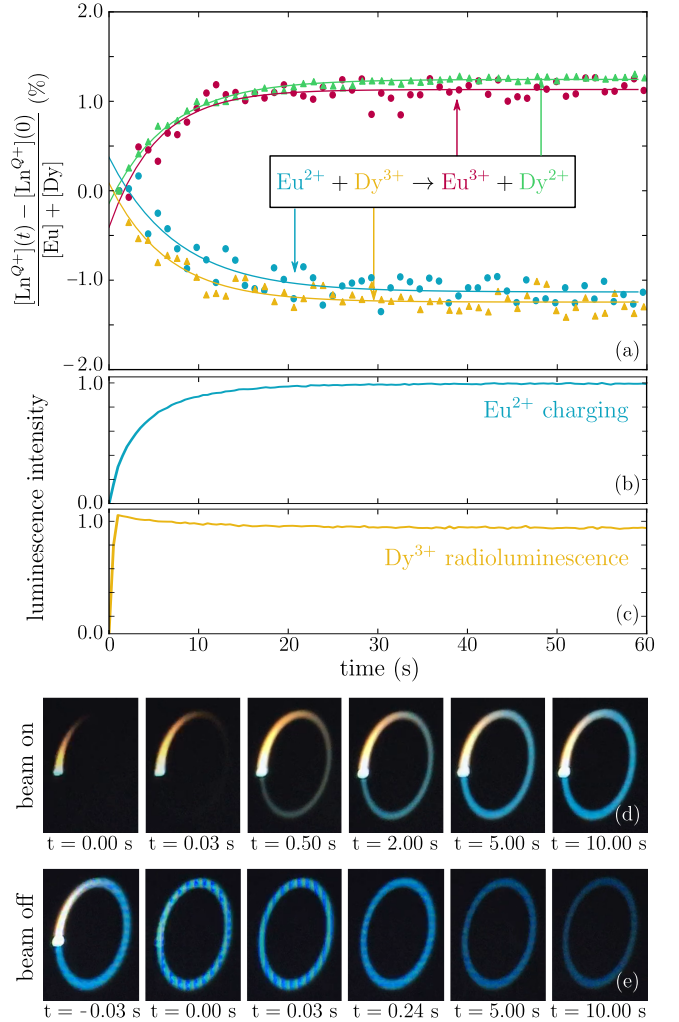


Figure 4 – Time evolution of the lanthanide oxidation states, relative to the total $[\text{Eu}]+[\text{Dy}]$ content from HERFD-XANES (a). Time $t = 0$ corresponds to switching on of the X-ray beam. Simultaneously, the radioluminescence is probed for Eu²⁺ (broad band emission in 450-550 nm range) (b) and Dy³⁺ (line emission in 550-600 nm range) (c). Pictures of the rotating sample illustrate the charging and afterglow of the blue Eu²⁺ emission when the beam is switched on (d) and off (e), respectively.

of magnitude as a prior estimate for the number of Eu ions changing valence state, based on optical spectroscopy experiments on $\text{SrAl}_2\text{O}_4:\text{Eu,Dy}$ ⁵⁵, suggesting that the found electron transfer is indeed related to the persistent luminescence.

In order to further substantiate the connection between the electron transfer and the persistent luminescence, their time evolution was measured. The result is shown in Fig. 4, where an optically cleaned phosphor, *i.e.* for which all traps were first emptied by OSL, is irradiated by the X-ray beam by opening the fast shutter at $t = 0$. The oxidation states of the lanthanide ions are sampled every 100 ms from the HERFD-XANES intensity at a fixed energy, corresponding to the white line maximum. From Fig. 4(a), it is clear that the X-ray induced oxidation of Eu^{2+} and reduction of Dy^{3+} occur on the same time scale of about 20 s. After this, a dynamic equilibrium is reached where the forward and backward electron transfers, Eq. 1, occur at the same rate. It should be noted that this relatively long time scale is the consequence of the sample being mounted on a rotating stage. If not, the dynamic equilibrium would have been reached after 0.1 s, presumably explaining why no valence state changes were found in prior investigations^{30–33,35}.

Figure 4(b) shows that the charging of the persistent luminescence under the experimental irradiation conditions follows indeed the same temporal behavior as the electron transfer. In contrast, the Dy^{3+} radioluminescence (RL), shown in Fig. 4(c), grows fast, in the 0.1–0.5 ms range, corresponding to the intrinsic rate of the inter- $4f^9$ transitions^{56,57}. In the same time frame of the charging, the Dy^{3+} RL intensity shows a small decrease, presumably due to the partial reduction of the Dy^{3+} ions.

The variations in luminescence are also visible in Fig. 4(d) showing the rotating sample at several time delays after switching on the X-ray beam. The coma shaped signature of the Dy^{3+} RL appears instantaneously, while the blue persistent luminescence builds up more slowly. Complementary, Fig. 4(e) displays how the Dy^{3+} RL disappears almost immediately after switching off the X-ray beam, leaving the blue afterglow visible for several hours. The first two frames of 4(e) confirm that the intensity of the blue Eu^{2+} luminescence that is probed during this experiment is due solely to the afterglow, *i.e.* the blue intensity along the rim of the pellet does not change abruptly when the excitation is switched off.

In summary, a dedicated RIXS study is performed on $\text{Sr}_4\text{Al}_{14}\text{O}_{25}:\text{Eu,Dy}$ persistent luminescent materials in order to elucidate the electron transfer that underlies the energy storage in this persistent phosphor. While the X-rays allow to accurately probe the oxidation states of both dopants in real time, they unavoidably disturb the equilibrium electron occupation, prohibiting the unambiguous assessment of the persistent luminescence mechanism unless measures are taken to overcome the beam effect. A novel measurement approach is demonstrated, where illumination with visible and near-IR light are used to manipulate the electron oc-

cupations, in combination with an effective method to spread the applied X-ray dose by rapidly spinning the sample. Excitation by violet light induces trapping, creating metastable $\text{Eu}^{3+}\text{-Dy}^{2+}$ centers, while IR light provokes detrapping, as described by Eq. 1. Quantitatively, 3% of the Eu ions and a corresponding number of Dy ions are affected, in agreement with the optically determined storage capacity. The characteristic time of the metastable $\text{Eu}^{3+}\text{-Dy}^{2+}$ state coincides with the charging of the persistent luminescence. This is hence the first confirmation of the popular, yet debated, model where Dy^{3+} acts as the main electron trap in persistent phosphors.

Acknowledgements

JJJ acknowledges the UGent Special Research Fund (BOF/PDO/2017/002101). We acknowledge the European Synchrotron Radiation Facility (ESRF) for the allocation of beamtime (beamline ID26).

References

- [1] J. W. Qiao, M. Amachraa, M. Molokeev, Y. C. Chuang, S. P. Ong, Q. Y. Zhang, and Z. G. Xia. Engineering of $\text{K}_3\text{YSi}_2\text{O}_7$ To Tune Photoluminescence with Selected Activators and Site Occupancy. *Chem. Mater.*, 31(18):7770–7778, 2019.
- [2] J. Qiao, G. Zhou, Y. Zhou, Q. Zhang, and Z. Xia. Divalent Europium-Doped Near-Infrared-Emitting Phosphor for Light-Emitting Diodes. *Nat. Commun.*, 10:5267, 2019.
- [3] T. Maldiney, A. Bessiere, J. Seguin, E. Teston, S. K. Sharma, B. Viana, A. J. J. Bos, P. Dorenbos, M. Bessodes, D. Gourier, D. Scherman, and C. Richard. The In Vivo Activation of Persistent Nanophosphors for Optical Imaging of Vascularization, Tumours and Grafted Cells. *Nat. Mater.*, 13(4):418–426, 2014.
- [4] D. Hayashi, A. M. van Dongen, J. Boerekamp, S. Spoor, G. Lucassen, and J. Schleipen. A Broadband LED Source in Visible to Short-Wave-Infrared Wavelengths for Spectral Tumor Diagnostics. *Appl. Phys. Lett.*, 110(23):233701, 2017.
- [5] V. Rajendran, M. H. Fang, G. N. De Guzman, T. Lesniewski, S. Mahlik, M. Grinberg, G. Leniec, S. M. Kaczmarek, Y. S. Lin, K. M. Lu, C. M. Lin, H. Chang, S. F. Hu, and R. S. Liu. Super Broadband Near-Infrared Phosphors with High Radiant Flux as Future Light Sources for Spectroscopy Applications. *ACS Energy Lett.*, 3(11):2679–2684, 2018.
- [6] E. Song, X. Jiang, Y. Zhou, Z. Lin, S. Ye, Z. Xia, and Q. Zhang. Heavy Mn^{2+} Doped MgAl_2O_4 Phosphor for High-Efficient Near-Infrared Light-Emitting Diode and the Night-Vision Application. *Adv. Opt. Mater.*, 7(24):1901105, 2019.

- [7] L. Zhang, D. Wang, Z. Hao, X. Zhang, G. Pan, H. Wu, and J. Zhang. Cr³⁺-Doped Broadband NIR Garnet Phosphor with Enhanced Luminescence and its Application in NIR Spectroscopy. *Adv. Opt. Mater.*, 7(12):1900185, 2019.
- [8] P. A. Jursinic. Characterization of Optically Stimulated Luminescent Dosimeters, OSLDs, for Clinical Dosimetric Measurements. *Med. Phys.*, 34(12):4594–4604, 2007.
- [9] E. G. Yukihara and S. W. S. McKeever. Optically Stimulated Luminescence (OSL) Dosimetry in Medicine. *Phys. Med. Biol.*, 53(20):R351–R379, 2008.
- [10] K. Van den Eeckhout, P. F. Smet, and D. Poelman. Persistent Luminescence in Eu²⁺-Doped Compounds: A Review. *Materials*, 3(4):2536–2566, 2010.
- [11] Y. Li, M. Gecevicius, and J. Qiu. Long Persistent Phosphors - From Fundamentals to Applications. *Chem. Soc. Rev.*, 45:2090–2136, 2016.
- [12] R. E. Rojas-Hernandez, F. Rubio-Marcos, M. Á. Rodriguez, and F. Fernandez. Long Lasting Phosphors: SrAl₂O₄:Eu, Dy as the Most Studied Material. *Renew. Sust. Energ. Rev.*, 81:2759 – 2770, 2018.
- [13] J. Xu and S. Tanabe. Persistent Luminescence Instead of Phosphorescence: History, Mechanism, and Perspective. *J. Lumin.*, 205:581–620, 2019.
- [14] A. J. J. Bos. Theory of thermoluminescence. *Radiat. Meas.*, 41:S45–S56, 2006.
- [15] K. Van den Eeckhout, A. J. J. Bos, D. Poelman, and P. F. Smet. Revealing Trap Depth Distributions in Persistent Phosphors. *Phys. Rev. B*, 87(4), 2013.
- [16] J. Botterman and P. F. Smet. Persistent Phosphor SrAl₂O₄:Eu,Dy in Outdoor Conditions: Saved by the Trap Distribution. *Opt. Express*, 23(15):A868–A881, 2015.
- [17] R. R. Petit, S. E. Michels, A. Feng, and P. F. Smet. Adding Memory to Pressure-Sensitive Phosphors. *Light: Sci. Appl.*, 8(124), 2019.
- [18] H. Terraschke, M. Franzreb, and C. Wickleder. Magnetism and Afterglow United: Synthesis of Novel Double Core-Shell Eu²⁺-doped Bifunctional Nanoparticles. *Chem.: Eur. J.*, Accepted, 2020.
- [19] T. Lécuyer, E. Teston, G. Ramirez-Garcia, T. Maldiney, B. Viana, J. Seguin, N. Mignet, D. Scherman, and C. Richard. Chemically Engineered Persistent Luminescence Nanoprobes for Bioimaging. *Theranostics*, 6(13):2488–2524, 2016.
- [20] L. Yan, L. Chen, X. Zhao, and X. Yan. pH Switchable Nanoplatfom for In Vivo Persistent Luminescence Imaging and Precise Photothermal Therapy of Bacterial Infection. *Adv. Funct. Mater.*, Accepted:1909042, 2020.
- [21] A. Harizaj, O. Q. De Clercq, B. Descamps, C. Vanhove, S. C. De Smedt, D. Poelman, I. Lentacker, and K. Braeckmans. Biocompatible Lipid-Coated Persistent Luminescent Nanoparticles for In Vivo Imaging of Dendritic Cell Migration. *Part. Part. Syst. Charact.*, 36(11):1900371, 2019.
- [22] E. M. Rodríguez, G. López-Peña, E. Montes, G. Lifante, J. G. Solé, D. Jaque, L. A. Diaz-Torres, and P. Salas. Persistent Luminescence Nanothermometers. *Appl. Phys. Lett.*, 111(8):081901, 2017.
- [23] T. Matsuzawa, Y. Aoki, N. Takeuchi, and Y. Murayama. New long phosphorescent phosphor with high brightness, SrAl₂O₄:Eu²⁺,Dy³⁺. *J. Electrochem. Soc.*, 143(8):2670–2673, 1996.
- [24] J. Cai, W. Jing, J. Cheng, Y. Zhang, Y. Chen, M. Yin, Y. Yeung, and C. Duan. First-Principles Calculations of Photoluminescence and Defect States of Ce³⁺-Doped (Ca/Sr)₂B₅O₉Cl. *Phys. Rev. B*, 99:125107, 2019.
- [25] Micah P. Prange, Niranjan Govind, and Sebastien N. Kerisit. *Ab Initio* Calculations of the Rate of Carrier Trapping and Release at Dopant Sites in NaI:Tl Beyond the Harmonic Approximation. *Phys. Rev. B*, 101:024304, 2020.
- [26] J. Botterman, J. J. Joos, and P. F. Smet. Trapping and detrapping in SrAl₂O₄:Eu,Dy persistent phosphors: Influence of excitation wavelength and temperature. *Phys. Rev. B*, 90(8):085147, 2014.
- [27] V. Laguta, M. Buryi, P. Arhipov, O. Sidletskiy, O. Laguta, M. G. Brik, and M. Nikl. Oxygen-Vacancy Donor-Electron Center in Y₃Al₅O₁₂ Garnet Crystals: Electron Paramagnetic Resonance and Dielectric Spectroscopy Study. *Phys. Rev. B*, 101:024106, 2020.
- [28] T. Delgado, S. Ajoubipour, J. Afshani, S. Yoon, B. Walfort, and H. Hagemann. Spectroscopic Properties of Dy³⁺- and Dy³⁺, B³⁺- doped SrAl₂O₄. *Opt. Mater.*, 89:268 – 275, 2019.
- [29] C. MacKeen, F. Bridges, L. Seijo, Z. Barandiarán, M. Kozina, A. Mehta, M. F. Reid, and J. P. R. Wells. The Complexity of the CaF₂:Yb System: A Huge, Reversible, X-ray-Induced Valence Reduction. *J. Phys. Chem. C*, 121(51):28435–28442, 2017.
- [30] Z. Qi, C. Shi, M. Liu, D. Zhou, X. Luo, J. Zhang, and Y. Xie. The Valence of Rare Earth Ions in R₂MgSi₂O₇:Eu, Dy (R = Ca, Sr) Long-Afterglow Phosphors. *Phys. Status Solidi A*, 201(14):3109–3112, 2004.

- [31] T. Aitasalo, J. Hassinen, J. Hölsä, T. Laamanen, M. Lastusaari, Malkamäki, J. Niittykoski, and P. Novák. Synchrotron Radiation Investigations of the $\text{Sr}_2\text{MgSi}_2\text{O}_7:\text{Eu}^{2+},\text{R}^{3+}$ Persistent Luminescence Materials. *J. Rare Earth*, 27(4):529 – 538, 2009.
- [32] S. Carlson, J. Hölsä, T. Laamanen, M. Lastusaari, M. Malkamäki, J. Niittykoski, and R. Valtonen. X-ray absorption study of rare earth ions in $\text{Sr}_2\text{MgSi}_2\text{O}_7:\text{Eu}^{2+},\text{R}^{3+}$ persistent luminescence materials. *Opt. Mater.*, 31(12):1877–1879, 2009.
- [33] J. Hölsä, T. Laamanen, M. Lastusaari, M. Malkamäki, E. Welter, and D. A. Zajac. Valence and Environment of Rare Earth Ions in $\text{CaAl}_2\text{O}_4:\text{Eu}^{2+},\text{R}^{3+}$ Persistent Luminescence Materials. *Spectrochim. Acta B*, 65(4):301–305, 2010.
- [34] K. Korthout, K. Van den Eeckhout, J. Botterman, S. Nikitenko, D. Poelman, and P. F. Smet. Luminescence and X-Ray Absorption Measurements of Persistent $\text{SrAl}_2\text{O}_4:\text{Eu},\text{Dy}$ Powders: Evidence for Valence State Changes. *Phys. Rev. B*, 84(8):085140, 2011.
- [35] M. Lastusaari, H. F. Brito, S. Carlson, J. Hölsä, T. Laamanen, L. C. V. Rodrigues, and E. Welter. Valences of Dopants in Eu^{2+} Persistent Luminescence Materials. *Phys. Scr.*, 89(4), 2014.
- [36] C. Gauthier, V. A. Sole, R. Signorato, J. Goulon, and E. Moguiline. The ESRF Beamline ID26: X-ray Absorption on Ultra Dilute Sample. *J. Synchrotron Radiat.*, 6:164–166, 1999.
- [37] P. Glatzel, T. C. Weng, K. Kvashnina, J. Swarbrick, M. Sikora, E. Gallo, N. Smolentsev, and R. A. Mori. Reflections on Hard X-Ray Photon-In/Photon-Out Spectroscopy for Electronic Structure Studies. *J. Electron Spectrosc.*, 188:17–25, 2013.
- [38] K. Hämäläinen, D. P. Siddons, J. B. Hastings, and L. E. Berman. Elimination of the Inner-Shell Lifetime Broadening in X-ray-Absorption Spectroscopy. *Phys. Rev. Lett.*, 67:2850–2853, 1991.
- [39] P. Carra, M. Fabrizio, and B. T. Thole. High Resolution X-Ray Resonant Raman Scattering. *Phys. Rev. Lett.*, 74:3700–3703, 1995.
- [40] P. Glatzel and U. Bergmann. High Resolution 1s Core Hole X-ray Spectroscopy in 3d Transition Metal Complexes - Electronic and Structural Information. *Coord. Chem. Rev.*, 249(1):65 – 95, 2005.
- [41] D. Dutczak, C. Ronda, T. Jüstel, and A. Meijerink. Anomalous Trapped Exciton and d-f Emission in $\text{Sr}_4\text{Al}_{14}\text{O}_{25}:\text{Eu}^{2+}$. *J. Phys. Chem. A*, 118(9):1617–1621, 2014.
- [42] D. Dutczak, T. Jüstel, C. Ronda, and A. Meijerink. Eu^{2+} Luminescence in Strontium Aluminates. *Phys. Chem. Chem. Phys.*, 17:15236–15249, 2015.
- [43] Z. Hu, G. Kaindl, and Meyer G. X-ray Absorption Near-Edge Structure at the L_{I-III} Thresholds of Pr, Nd, Sm, and Dy Compounds with Unusual Valences. *J. Alloys Compd.*, 246(1):186 – 192, 1997.
- [44] M. E. Fieser, M. G. Ferrier, J. Su, E. Batista, S. K. Cary, J. W. Engle, W. J. Evans, J. S. Lezama Pacheco, S. A. Kozimor, A. C. Olson, A. J. Ryan, B. W. Stein, G. L. Wagner, D. H. Woen, T. Vitova, and P. Yang. Evaluating the Electronic Structure of Formal Ln^{II} ions in $\text{Ln}^{II}(\text{C}_5\text{H}_4\text{SiMe}_3)_3^{1-}$ Using XANES Spectroscopy and DFT Calculations. *Chem. Sci.*, 8:6076–6091, 2017.
- [45] L. Amidani, K. Korthout, J. J. Joos, M. van der Linden, H. F. Sijbom, A. Meijerink, D. Poelman, P. F. Smet, and P. Glatzel. Oxidation and Luminescence Quenching of Europium in $\text{BaMgAl}_{10}\text{O}_{17}$ Blue Phosphors. *Chem. Mater.*, 29(23):10122–10129, 2017.
- [46] J. F. Herbst and J. W. Wilkins. Relativistic Calculations of $2p$ Excitation Energies in the Rare-Earth Metals. *Phys. Rev. B*, 26:1689–1701, 1982.
- [47] A. V. Soldatov, T. S. Ivanchenko, S. Della Longa, A. Kotani, Y. Iwamoto, and A. Bianconi. Crystal-Structure Effects in the Ce L_3 -Edge X-Ray-Absorption Spectrum of CeO_2 : Multiple-Scattering Resonances and Many-Body Final States. *Phys. Rev. B*, 50:5074–5080, 1994.
- [48] S. Tanaka, K. Okada, and A. Kotani. Resonant X-Ray Emission Spectroscopy in Dy Compounds. *J. Phys. Soc. Jpn.*, 63(7):2780–2787, 1994.
- [49] F. Bartolomé, J. M. Tonnerre, L. Sève, D. Raoux, J. Chaboy, L. M. García, M. Krisch, and C. C. Kao. Identification of Quadrupolar Excitation Channels at the L_3 Edge of Rare-Earth Compounds. *Phys. Rev. Lett.*, 79:3775–3778, 1997.
- [50] M. Nakazawa, K. Fukui, H. Ogasawara, A. Kotani, and C. F. Hague. X-Ray Absorption and Resonant X-Ray Emission Spectra by Electric Quadrupole Excitation in Light Rare-Earth Systems. *Phys. Rev. B*, 66:113104, 2002.
- [51] J. Prietzel, A. Botzaki, N. Tyufekchieva, M. Brettholle, J. Thieme, and W. Klysubun. Sulfur Speciation in Soil by S K-Edge XANES Spectroscopy: Comparison of Spectral Deconvolution and Linear Combination Fitting. *Environ. Sci. Technol.*, 45(7):2878–2886, 2011.
- [52] G. S. Henderson, F. M. F. de Groot, and B. J. A. Moulton. X-ray Absorption Near-Edge Structure (XANES) Spectroscopy. *Rev. Mineral. Geochem.*, 78(1):75–138, 2014.

- [53] G. Bunker. *Introduction to XAFS: A Practical Guide to X-ray Absorption Fine Structure Spectroscopy*. Cambridge University Press, 2010.
- [54] R. H. Packwood and J. D. Brown. A Gaussian Expression to Describe $\phi(\rho z)$ Curves for Quantitative Electron Probe Microanalysis. *X-Ray Spectrom.*, 10(3):138–146, 1981.
- [55] D. Van der Heggen, J. J. Joos, D. C. R. Burbano, J. A. Capobianco, and P. F. Smet. Counting the Photons: Determining the Absolute Storage Capacity of Persistent Phosphors. *Materials*, 10(8):867, 2017.
- [56] V. L. Levshin, N. D. Maksimova, and I. K. Lyubavskaya. Radiation Spectrum of Dy^{3+} in Y_2O_3 . *J. Appl. Spectrosc.*, 13:1035–1040, 1970.
- [57] E. Cavalli, M. Bettinelli, A. Belletti, and A. Speghini. Optical Spectra of Yttrium Phosphate and Yttrium Vanadate Single Crystals Activated with Dy^{3+} . *J. Alloys Compd.*, 341(1):107 – 110, 2002.